AGU PUBLICATIONS

JGR

Journal of Geophysical Research: Space Physics

RESEARCH ARTICLE
10.1002/2017JA024148

This article is a companion to *Bagenal et al.* [2017] doi:10.1002/2016JA023797 and 2017JA024053R.

Key Points:
- Protons comprise 1-20% of the plasma between 5 and 30 R_J
- Na^+ ions are detected between 5 and 40 R_J at an abundance of 1 to 10%
- SO_2^+ ions are detected between 5.31 and 5.07 R_J at an abundance of 0.1-0.6%

Correspondence to:
F. Bagenal,
bagenal@colorado.edu

Citation:
Bodisch, K. M., L. P. Dougherty, and F. Bagenal (2017), Survey of Voyager plasma science ions at Jupiter: 3. Protons and minor ions, *J. Geophys. Res. Space Physics*, *122*, doi:10.1002/2017JA024148.

Received 14 MAR 2017
Accepted 23 MAY 2017
Accepted article online 30 MAY 2017

©2017. American Geophysical Union. All Rights Reserved.

Survey of Voyager plasma science ions at Jupiter: 3. Protons and minor ions

K. M. Bodisch[1], L. P. Dougherty[1], and F. Bagenal[1]

[1]Laboratory for Atmospheric and Space Physics, University of Colorado Boulder, Boulder, Colorado, USA

Abstract When the Voyager 1 and 2 spacecraft flew through the Jovian system in March and July 1979, the Plasma Science instruments measured ions and electrons in the Io plasma torus and plasma sheet between 4.9 and 42 R_J. The dominant ions in the Jovian magnetosphere comprise the first few ionization states of atomic sulfur and oxygen. We present here an analysis of minor ion species H^+, Na^+, and SO_2^+. Protons are 1–20% of the plasma between 5 and 30 R_J with variable temperatures ranging by a factor of 10 warmer or colder than the heavy ions. We suggest that these protons, measured deep inside the magnetosphere, are consistent with a source from the ionosphere of ~$1.5–7.5 \times 10^{27}$ protons s^{-1} (2.5–13 kg/s). Na^+ ions are detected between 5 and 40 R_J at an abundance of 1 to 10%, produced by the ionization of the extended neutral cloud emanating from Io that has been observed since 1974. SO_2^+ ions are detected between 5.31 and 5.07 R_J at an abundance of 0.1–0.6%. These ions clearly come from the plasma interaction with Io's atmosphere, but the exact processes whereby atmospheric molecules escape Io and end up as ions well inside Io's orbit are not clear.

1. Introduction

In a series of three companion papers we present a reanalysis of Voyager 1 and 2 Plasma Science (PLS) data obtained at Jupiter in March and July 1979, respectively. In *Bagenal et al.* [2017], hereafter called Paper 1, we summarize the data and our analysis technique. In *Dougherty et al.* [2017], hereafter called Paper 2, we present the ion composition found in different regions of the Jovian plasma disk. In this third paper we discuss the distribution of protons (H^+) and other minor ion species (Na^+ and SO_2^+).

Paper 1 includes figures illustrating the trajectories of the Voyager spacecraft through the Jovian system. To summarize: in March and July of 1979 the Voyager 1 and Voyager 2 spacecraft approached at late morning local time, getting closest to Jupiter at dusk, then departing in the early morning sector. Voyager 2's closest approach of ~10 R_J (radius of Jupiter = 71,492 km) was outside Europa's orbit, while Voyager 1 reached 4.9 R_J, inside the Io torus. The plasma seemed a little hotter on the Voyager 2 pass and the spectral peaks (for different ion species moving at the same bulk speed) were not so distinct. Like previous analyses, we focus on PLS data taken by Voyager 1.

Each of the Voyager spacecraft carries a set of Faraday cups, the main three of which (A, B, and C cups) measure ions, a fourth (side-pointing) (D cup) measures both ions and electrons in the energy-per-change (E/Q) range of 10 to 5950 V [*Bridge et al.*, 1977]. The higher-resolution mode has 128 channels logarithmically space with $\Delta E/E \sim 3.6\%$. The PLS observations of electrons at Jupiter are discussed by *Scudder et al.* [1981] and *Sittler and Strobel* [1987]. Paper 1 presents a full description of the Voyager PLS instrument, a review of previous analyses of the ion data at Jupiter, a summary of our reanalysis techniques, and presents the derived plasma parameters versus time along the spacecraft trajectory.

In Paper 2 we present the plasma properties of the heavy ions versus radial distance. The main results of Paper 2 are the following: (1) the plasma sheet shows a relative uniform structure of decreasing electron density (N_e) and increasing temperature out to ~20 R_J and beyond ~15 R_J there is increasing disorder with sporadic blobs of cold plasma; (2) The fraction of suprathermal (100 eV) ions increases with distance to over 50% beyond ~9 R_J; (3) The ion composition in the cold blobs is consistent with the ion abundances derived from physical chemistry models extending from 6 to ~9 R_J where the collisional reactions slow down and radial transport speeds up, effectively freezing in the ion composition to the following abundances: O^+/N_e = 15–22%, S^{++}/N_e = 10–19%, O^{++}/N_e = 4–8%, S^{+++}/N_e = 4–6%, and S^+/N_e = 1–5% which is similar to the composition derived by *Delamere et al.* [2005] from a physical chemistry model constrained by Cassini Ultraviolet Imaging Spectrograph (UVIS) observations.

Protons appear regularly throughout the magnetosphere of Jupiter. The Voyager PLS instrument separates ion species that are comoving by their mass-per-charge (M/Q). *McNutt et al.* [1981] used the M/Q = 1 peak in the energy/charge spectrum to confirm the bulk plasma flow speed and show the deviation from corotation in the plasma sheet (10–42 R_J). *Bagenal* [1985] reported proton densities in the cold inner torus (<5 R_J). Otherwise, Voyager PLS studies to date have focused on the heavy ions. Unlike the dissociation products of SO_2 from Io's volcanoes, there are multiple potential sources of protons: the solar wind, the ionosphere of Jupiter, and/or dissociation and ionization of water from the icy moons. *Nagy et al.* [1986] made an early estimate of the ionospheric source (35 kg/s) of which an update is long overdue. *Hill et al.* [1983] estimated the solar wind source to be 20 kg/s. *Bagenal and Delamere* [2011] bumped this up to 150 kg/s. Otherwise, protons have basically been ignored. A goal of this paper is to map out the spatial distribution of the properties of protons in the Jovian magnetosphere with the hope that these properties will elucidate their origins. We compare our results with proton measurements made at higher energies by Voyager, Ulysses and Galileo.

The detection of optical emission from neutral atoms of sodium near Io by *Brown* [1974] was the first indication that Io might provide a source of plasma to the magnetosphere. These ground-based observations of Na around Io revealed an extended neutral cloud [*Trafton et al.*, 1974]. The first spectral identification of sodium in an ionized state came in a tentative report by *Hall et al.* [1994] of emission near 372 Å in the emission spectrum of the torus obtained by the Earth-orbiting EUVE satellite. *McNutt* [1993] makes the case for detection of Na^+ ions in a Voyager PLS measurement at 42 R_J. Earlier analysis of the Voyager PLS data in the cold torus by *Bagenal and Sullivan* [1981] and *Bagenal* [1985] reported an upper limit of the abundance of Na^+ ions at 3%. In this paper we present the positive identification of in situ Na^+ at several places between 4.9 and 42 R_J in the Voyager PLS data.

Sulfur dioxide was detected spectroscopically by the Voyager infrared interferometer spectrometer experiment on the surface of Io as frost [*Smythe et al.*, 1979] and as a gas in the atmosphere [*Pearl et al.*, 1979]. But the expectation was that little of the gas escaped Io and if it did the SO_2 would be quickly dissociated [*Shemansky*, 1980]. *Bagenal and Sullivan* [1981] and *Bagenal* [1985] recognized a M/Q = 64 peak in the Voyager PLS at 5.3 R_J, well inside Io's orbit (at 5.90 ± 0.02 R_J). In this paper, we summarize the observational evidence of SO_2^+ ions in the PLS data and discuss how these measurements fit into current understanding of the plasma interaction with Io's atmosphere.

In section 2 of this paper we present examples of the Voyager PLS data that illustrate how we measure H^+, Na^+, and SO_2^+ ions. In section 3 we show the radial distribution of H^+ and Na^+ ions and calculate the distribution of protons along the magnetic field to make 2-D maps. In section 4 we discuss the possible sources of H^+, Na^+, and SO_2^+ ions and present our conclusions in section 5.

2. Data Analysis

In paper 1 we described how we analyzed the Voyager PLS ion data by fitting each E/Q spectrum with a convected Maxwellian function for each species. When ions have a common bulk motion (as usual in magnetospheric plasmas) then the average, convective motion of each ion species produces a separate peak in an E/Q spectrum. If the ions are cold (i.e., the Mach number of the flow is high with the thermal or sound speed much less than the bulk motion) then the spread around the convective energy is small and the ion species is well resolved in the E/Q spectrum. On the other hand, if the ion species have a thermal speed comparable to the bulk motion, then the spectral peaks overlap. Depending on how well the spectral peaks were resolved, we made various assumptions about the temperature, flow, and/or composition.

Applying a physical chemistry model between 6 and 9 R_J, *Delamere et al.* [2005] derived the mixing ratios for the primary charge states of oxygen and sulfur ions which reached (>9 R_J) asymptotic values in the plasma sheet of the following: $N(O^+)/N_e$ = 20%; $N(O^{++})/N_e$ = 7%; $N(S^+)/N_e$ = 3%; $N(S^{++})/N_e$ = 17%; and $N(S^{+++})/N_e$ = 7% (allowing for ~10% of the charge as protons). We take the *Delamere et al.* [2005] composition to be our standard ion composition beyond 6 R_J. The electron density (N_e) is assumed to be equivalent to the total charge density derived from all the ion species fit to the PLS ion data. In Paper 2 we discuss the properties of heavy ions from 4.9 to 42 R_J including places where the composition deviates from the standard composition. Here we focus on the determination of proton properties at lower energy-per-charge (E/Q) and on the rare occasions where the spectrum can be fit at M/Q = 23 for Na^+ or M/Q = 64 for SO_2^+.

Table 1. Plasma Parameters Associated With the Cases of Positive H^+ Identification Shown in Figure 1

Time	*Delamere et al.* [2005]	63–15:24	63–19:56	63–23:24	64–01:42	64–11:48
Figure		Figure 1a	Figure 1b	Figure 1c	Figure 1d	Figure 1e
Focus ion		H^+	H^+	H^+	H^+	H^+
R_J	>9 R_J	19.93	16.32	13.50	11.60	4.89
N_e		1.4	5.2	14	31	220
		±8%	±5%	±2%	±1%	±0.4%
H^+		0.28	0.66	1.1	2.7	4.9
		±34%	±25%	±3%		
%	10	20	13	7.8	8.6	2.3
O^{++}		0.1	0.76	0.84	2.8	41
		±15%	±7%	±3%	±1%	±1%
%	7	7.3	15	5.8	9	19
O^+		0.17	0.52	2.2	5.6	84
		±15%	±7%	±3%	±1%	±1%
%	20	12	10	16	18	39
S^{+++}		0.05	0.24	0.83	1.4	1.8
		±15%	±7%	±3%	±1%	±7%
%	7	3.9	4.7	5.7	4.5	.84
S^{++}		0.14	0.43	1.9	4.7	8.5
		±15%	±7%	±3%	±1%	±1%
%	17	13	8.4	13	15	3.9
S^+			0.066	0.60	0.84	5.9
			±7%	±3%	±1%	
%	3		1.2		2.7	2.7
O^+ hot		0.25	0.7	2.2	1.6	15.3
%		18	14	15	5.2	7
Na^+		0.042	0.083	0.36	1.2	2.22
		±200%	±7%	±3%	±1%	±11%
%		3.0	1.6	2.5	3.8	1
$T(H^+)$		5.1	34.7	24.9	15	2.08
		±85%	±60%	±10%		
T_i		62	187	24.9	24.3	0.72
		±45%	±35%	±10%	±5%	±1%
T_{hot}		900	900	750	600	69
V_{phi}		212	183	135	113	61.8
		±2%	±2%	±0.4%	±0.3%	±0.04%
V_{phi}/V_{co}		0.85	0.9	0.79	0.77	1

Fit parameters are shown in black with the corresponding percentage uncertainties shown in green. Units: Densities are in cm^{-3}; temperatures are eV; velocities are in km/s; abundances (blue) are $N_i/N_e \times 100$. The first column gives the percentage abundance from the physical chemistry model of *Delamere et al.* [2005] matched to the Cassini UVIS observations of *Steffl et al.* [2004].

2.1. Fit Cases

We describe in Paper 1 five primary types of cases used to match the heavy ions properties to the PLS ion data. Sometimes, we can allow the fitting code to find the best fit of a clear spectral peak. For the minor ion species often we often needed to hand adjust the fits. When the plasma is hot and the spectral peaks merge, we need to make several assumptions to fit the spectrum.

Paper 1 describes (and illustrates with examples) the five types of circumstances (cases i to v) that were used to fit the heavy ion peaks in the PLS spectra.

1. case i (blue)—variation of all parameters (mostly in the inner cold torus);
2. case ii (red)—constraining the ion abundances of the five main ion species (O^+, O^{++}, S^+, S^{++}, and S^{+++}) to the standard composition based on *Delamere et al.* [2005] as listed in Table 1;
3. case iii (black)—fixed ion composition plus fixed flow speed;
4. case iv (green)—cold blobs in the plasma sheet where resolved peaks can be fit allowing some variation in composition;
5. case v (purple)—interpolation between the composition of the cold torus and the standard composition at 6 R_J from *Delamere et al.* [2005].

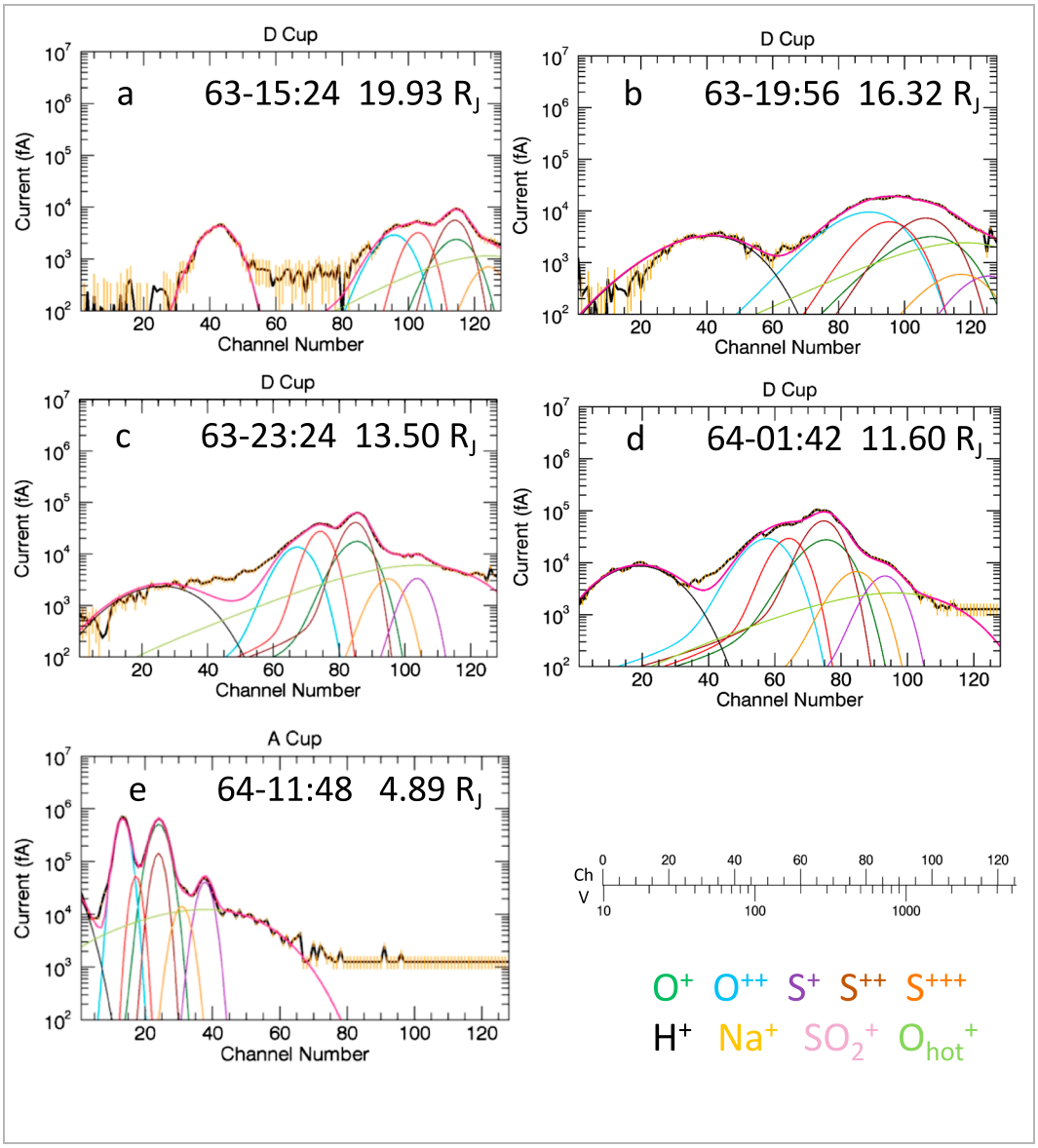

Figure 1. Five cases of positive identification of H^+ ions. (a–d) The spectra are from the (side) D cup. (e) The spectrum is from the (main) A cup. The parameters from fitting these spectra are given in Table 1. Bottom right are the colors of the that are fit to the spectra plus the conversion scale from channel number (Ch) to energy/charge (V). The vertical scale is in fempto-Amps (fA) from 10^2 to 10^7 fA. The black line shows the data with measurement errors shown in orange. The sum of currents due to the different ion species is shown in red.

Protons. While there were some Voyager 1 spectra as far from Jupiter as 42 R_J where heavy ions could be distinguished, a distinct peak at lower E/Q for protons was only occasionally seen between 20 and 30 R_J and was most often observed inside 20 R_J. Figure 1 shows five examples of spectra to illustrate the sorts of situations where we can fit a proton peak. The corresponding plasma parameters are listed in Table 1 with the *Delamere et al.* [2005] composition for comparison. Figure 1a shows an example from just inside 20 R_J where comoving protons and heavy ions are clearly resolved, moving at 85% of corotation. On this occasion, the protons are considerably colder (5.1 eV) than the heavy ions (62 eV) which have a modified standard composition. Figure 1b shows an example where the plasma is warmer (though the protons still remain colder than the heavy ions), and the composition is modified from standard with a high O^{++} composition. Figures 1c and 1d are examples at 13.5 and 11.6 R_J where the protons are less and more prominent, respectively. Where

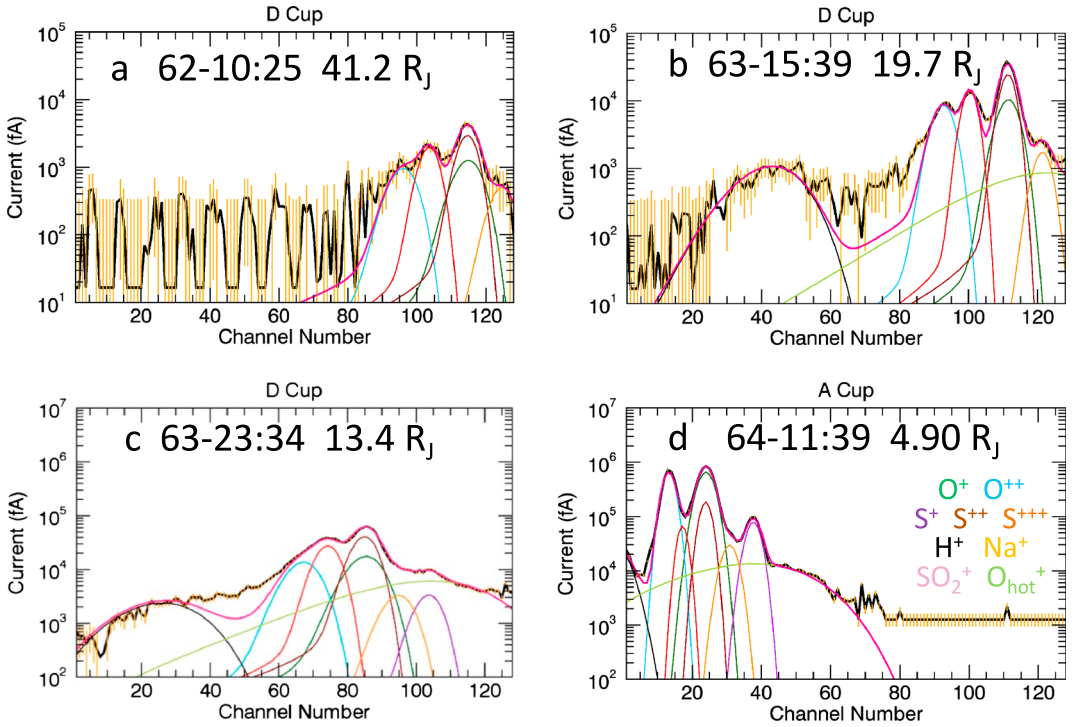

Figure 2. Four cases of positive identification of Na^+ ions. The parameters from fitting these spectra are given in Table 2. (a–c) The spectra are from the (side) D cup. (d) The spectrum is from the (main) A cup. See Figure 1 caption for description of spectra.

the proton peak is distinct (Figure 1d), we can fit the spectral feature to get density and temperature. At other times (Figure 1c), the proton peak is not distinct and we fix the proton temperature to be the same as the heavy ions (also see examples in Figures 3c and 3d in Paper 1). In the cold inner torus where the corotation speed has dropped to ~60 km/s the proton peak falls below the 10 eV lower limit of the PLS instrument. For these instances there is a clear shoulder to the spectrum (seen best in the A Cup spectrum shown in Figure 2d) covering at least five channels as illustrated in Figure 1e. The temperature of these protons (~2 eV) seems to be a little higher than the very cold (0.7 eV) heavy ions. Few Voyager 2 spectra have resolvable peaks and, at best, look similar to Figure 1b. The heavies were assumed to have the standard composition.

Sodium. Figure 2 shows examples of the very few spectra where there is a distinct feature corresponding to Na^+ ions at M/Q = 23. The left side of Table 2 gives the plasma properties for these cases. More often, the Na^+ abundance is determined by fitting the spectrum between peaks at M/Q = 16 and 32. The Na^+ peak is never distinct enough to determine the temperature, and we assume that the sodium ions have the same temperature as the other heavy ions. Abundances of sodium ions were determined between 41 and 4.9 R_J in the range of 1 to 10% of the local electron density.

Sulfur Dioxide. Figure 3 shows two examples of spectra where there is a distinct peak at M/Q = 64, which we assume to be SO_2^+ ions. The right side of Table 2 presents the plasma parameters associated with the fits shown in Figure 3. Such spectra are only found in the cold torus between 5.30 and 5.08 R_J. Again, there is not sufficient information to determine separate temperatures for the SO_2^+ ions, and we assume that these SO_2^+ ions have the same temperature as the heavy ion species. The abundance of these molecular ions is less than 1% of the electron density. *Bagenal* [1985] fit these same spectra (using a simple instrument response) with SO_2^+ ions and found similar parameters. The more sophisticated instrument response used in this reanalysis (discussed in Paper 1) probably does not make much difference at the very high Mach plasma conditions in the cold torus. The main difference in the current analysis is the inclusion of hot ions (80–100 eV, assumed here to be O^+) at an abundance of a few percent which fills the spectrum at energies above the main peaks. *Bagenal* [1985] examined the options of increasing the temperature of SO_2^+ ions (to 6 eV) or adding small amounts of SO^+ and SO_3^+ ions. We return to these molecular ions in section 4.

Table 2. Plasma Parameters Associated With the Cases of Positive Na^+ and SO_2^+ Identification Shown in Figure 2

Time	62–10:25	63–14:39	63–23:34	64–11:39	64–10:09	64–10:49
Figure	Figure 2a	Figure 2b	Figure 2c	Figure 2d	Figure 3a	Figure 3b
Focus ion	Na^+	Na^+	Na^+	Na^+	SO_2^+	SO_2^+
R_J	41.2	19.7	13.4	4.90	5.31	5.07
N_e	0.34	2.3	14	260	1537	1230
	±22%	±5%	±2%		±0.05%	±0.03%
H^+		0.14	0.65	4.8	4.0	5.1
		±80%	±3%		±45%	
%		5.8	4.6	1.9	0.25	0.41
O^{++}	0.026	0.18	0.81	41	17	31
	±22%	±5%	±3%	±1%	±3.0%	±2%
%	7.7	7.6	5.8	16	1.0	2.5
O^+	0.071	0.43	2.2	110	324	375
	±22%	±5%	±3%	±1%	±2%	±1%
%	21	19	15	43	20	30
S^{+++}	0.026	0.14	0.80	2.3	3.2	3.9
	±22%	±5%	±3%	±7%	±2%	9%
%	7.6	6	5.7	0.88	0.2	0.31
S^{++}	0.059	0.36	1.8	11	32	38
	±22%		±3%	±1%	±2%	±1%
%	17	16	13	4.3	2.1	3
S^+			0.30	11	1020	628
			±3%	±2%	±2%	±1%
%				4.4	64	51
O^+_{hot}		0.2	2.9	17	60	27
%		8.6	21	6.4	4	2
Na^+	0.024	0.06	0.35	4.7	64	49
	±180%	±95%	±3%	±6%	±18%	±5%
%	6.9	2.6	2.5	1.8	4	4
SO_2^+					9.3	1.6
					±4%	
%					0.58	0.13
$T(H^+)$		18.4	20.9	2.88	3.45	4.39
		±13%	±9%			
T_i	35.8	18.4	20.8	0.74	3.45	1.16
	±56%	±13%	±9%	±1%	±1.6%	±1%
T_{hot}		900	750	69	100	85
V_{phi}	216.2	204	132.5	61.6	66.7	63.4
	±2%	±0.3%	±0.4%	±0.04%	±0.1%	±0.03%
V_{phi}/V_{co}	0.42	0.82	0.78	1	1	1

Units: Densities are in cm^{-3}; temperatures are eV; velocities are in km/s; abundances are $N_i/N_e \times 100$.

2.2. Radial Profiles of Proton Density and Temperature

In Figure 4 we show the radial profiles of proton density, temperature, and percentage abundance ($N(H^+)/N_e \times 100$). Both densities (top) and temperatures (middle) derived from Voyager 1 inbound and outbound are shown in black and gray, respectively. The few Voyager 2 points (all >10 R_J) are shown in red brown. For the temperature profile, the dots show the proton temperature. We use crosses for the points where the heavy ion temperature was different from the proton temperature (shown with dots). The error bars in these fit parameters are shown in Figures 4 and 5 of Paper 1. The percent uncertainties for the fit parameters of the cases shown in Figure 1 are given in Table 1 (green numbers).

The density of protons shows a steady decline from ~80 cm^{-3} at 6 R_J to ~0.01 cm^{-3} at 25 R_J. The red-brown dots show that during the Voyager 2 flyby the density of protons 15–25 R_J was about a factor 5–10 higher and sometimes (e.g., at ~17 R_J) colder (red-brown dots) than the Voyager 1 epoch. The relative abundance of protons increases from a few percent at 6 R_J to 10–20% at ~10 R_J and remains at about that level to beyond 25 R_J. The large variations in temperature—both within and between the protons and heavies—between 10 and 25 R_J is consistent with the present of small blobs of cold plasma reported in Paper 2. Figure 4 (bottom) shows that the abundance of protons does not vary greatly in such blobs, but Figure 4 (middle) shows that the temperature of the protons can be very different from the heavy ions, indicating a different heating/cooling

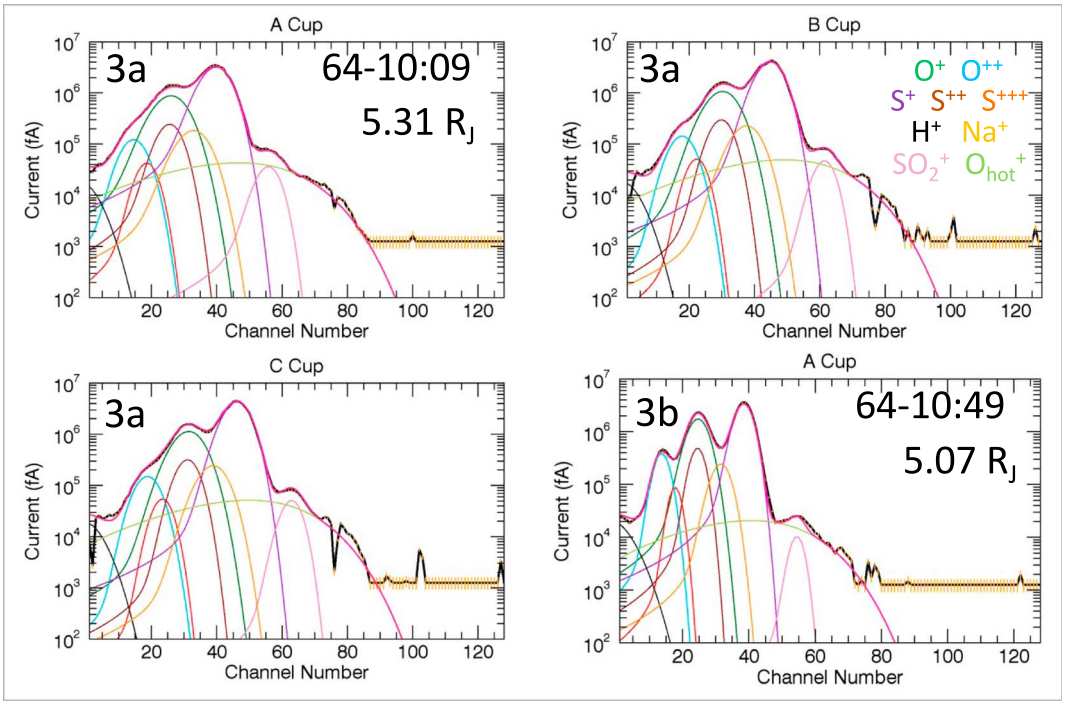

Figure 3. Two cases of positive identification of SO_2^+ ions. (a) The fit to all three cups of the main sensor at the time of the farthest encounter of a detectable peak at M/Q = 64. (b) The last occasion of a distinct M/Q = 64 peak (A Cup only). The parameters from fitting these spectra are given in Table 2. See Figure 1 caption for description of spectra.

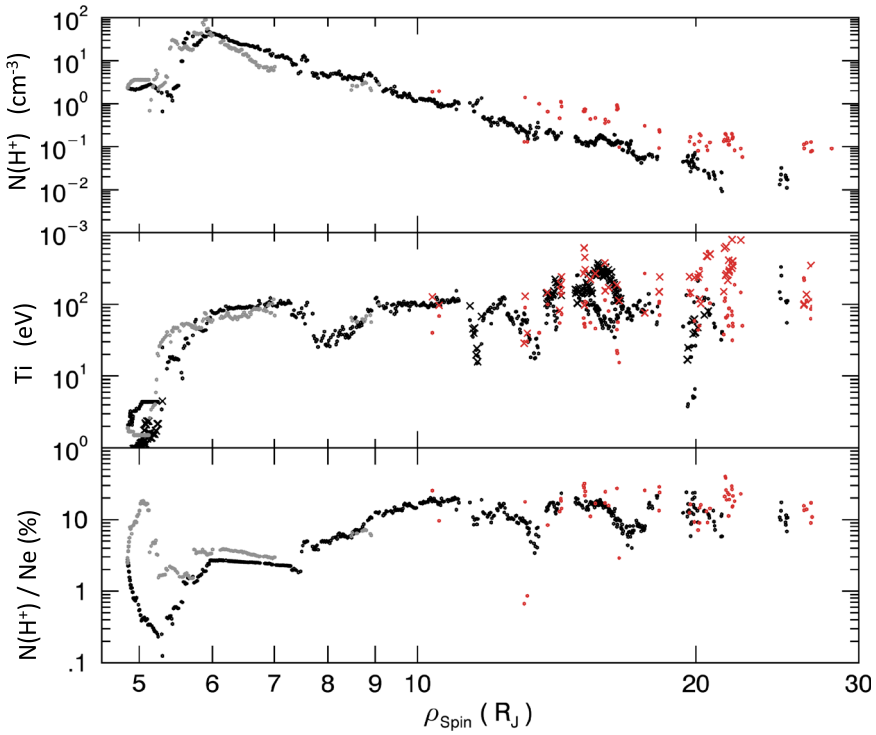

Figure 4. Radial profiles of (top) proton density, (middle) temperature, and (bottom) percent abundance for Voyager 1 inbound (black), Voyager 1 outbound (gray), and Voyager 2 (red brown). Where the proton temperatures are the same as the heavy ions they are shown as black, gray, and red-brown dots. The places where the heavy ion temperatures are different from the protons are shown as crosses.

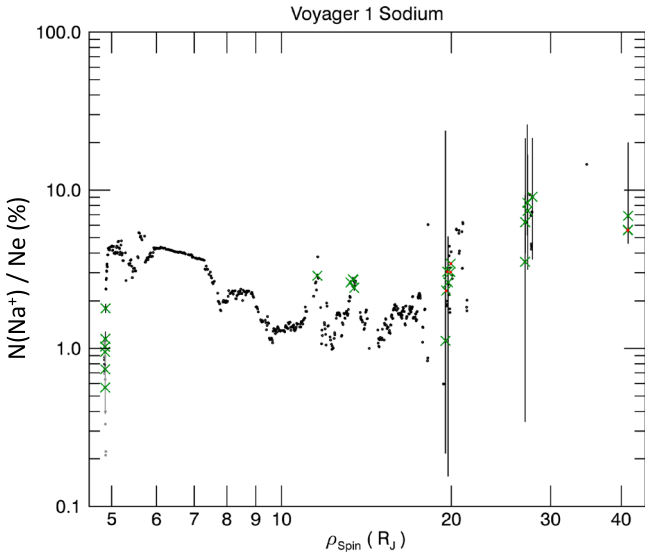

Figure 5. Radial profile of the percent abundance of sodium. The green crosses are places where there is a detectable feature in the spectrum at M/Q = 23. The error bars indicate the uncertainties in the fit parameters for these particular points. There are few cases (red dots) where the error bars were particularly large (>100%).

history between protons and heavies. Sometimes (e.g., Figures 1a and 1b), the protons are much colder than the heavies. But at other times, particularly for Voyager 2, the protons are much colder than the heavy ions.

Finally, we point out that inside 6 R_J the plasma is much colder and the heavy ions are more tightly confined to the equator. The ambipolar electric field (see section 3) pulls the protons off the centrifugal equator so that the large variations in local proton abundance inbound (black) and outbound (gray) in Figure 4 (bottom) inside 6 R_J is likely mostly latitude dependence. In a future study, we plan to calculate the total flux tube content of protons which we expect to be a better indication of true proton abundance in the cold, inner torus.

2.3. Radial Profile of Sodium Density

Figure 5 is the radial profile of the percent abundance of sodium ions, $N(Na^+)/N_e \times 100$, in the Voyager 1 PLS data (we did not find distinct evidence of Na^+ in the Voyager 2 data). For most cases (black dots) the density of the sodium ions is fixed to be ~16% of the O^+ density. The green crosses mark areas where there is a distinct feature in the spectrum that we can associate with a M/Q = 23 ion. The error bars show the uncertainties in the abundance derived for these cases, except on a few occasions (red dots) where the formal uncertainties were >100%. The percent uncertainties for the specific cases shown in Figure 2 are listed in Table 2. The values of the sodium abundance range from a little under 1% to nearly 10%.

In the warm torus (>6 R_J) and beyond it is not clear if the factor ~5 variability in the sodium abundance is real. In the cold inner torus (<6 R_J) the sharp drop in the sodium abundance may reflect latitudinal variations and/or may be related to distance from the Io neutral sodium corona.

2.4. Distribution of Sulfur Dioxide Ions

There are about 20 spectra obtained on the Voyager 1 inbound pass in the cold inner torus, between 5.31 and 5.07 R_J (when the spacecraft was very close to the centrifugal equator) where a distinct peak is visible in the

Table 3. Empirical Power Law Functions for Proton Density Radial Profile at the Centrifugal Equator Beyond 6 R_J[a]

Regime	Formula		
B&D 2011	$N_{2011}(R) = 1987\ (R/6)^{-8.2} + 14\ (R/6)^{-3.2} + 0.05\ (R/6)^{-0.65}$		
$6 \le R \le 15.2$	$N(R) = a\ (R/6)^b$		
$R > 15.2$	$N(R) = c\ n_{2011}(R)$		
Parmeter	a	b	c
Value	50.6	−5.31	0.212

[a]All densities are in units of cm^{-3}. B&D 2011 refers to the electron density profile of *Bagenal and Delamere* [2011].

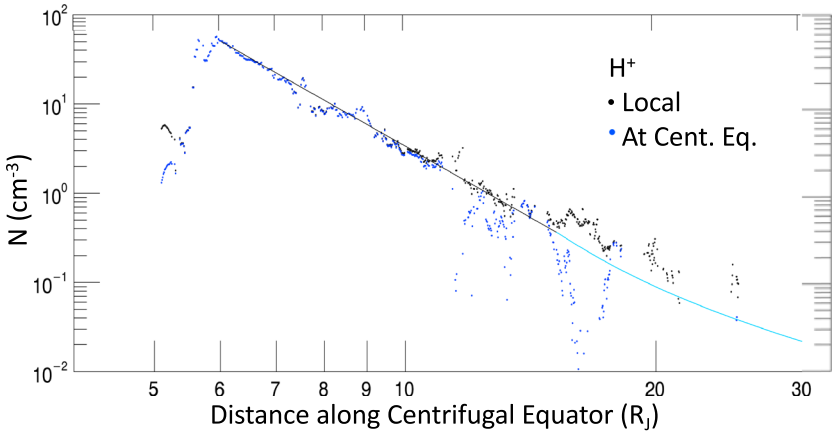

Figure 6. Radial profiles of density measured at the spacecraft and extrapolated to the centrifugal equator of H^+ with empirical functions for >6 R_J. Values for the power law functions are given in Table 3.

spectrum at M/Q = 64. The first and last of these spectra are shown in Figure 3, and the values of the fit parameters are shown in Table 3. We fit the spectra with the same temperature for SO_2^+ as the rest of the heavy ions. The local densities range from 1.6 to 9.3 cm^{-3}, corresponding to abundances of SO_2^+ ions in the range 0.1% to 0.6% of the local electron density.

3. Spatial (2-D) Distribution

Figures 4 and 5 show the densities of protons and sodium ions at the location of the spacecraft. The spacecraft trajectory was close to the Jovigraphic equator (see Figure 1 of Paper 2). Jupiter's magnetic field is tilted nearly 10° from the planet's spin axis so that the plasma disk moved across the spacecraft twice per 10 h spin period. In a rotation-dominated magnetosphere the plasma is centered on the centrifugal equator, the point along the magnetic field that is farthest from the spin axis. The ions (particularly heavier species) feel a strong centrifugal force toward the equator, while the electrons are more spread out. An ambipolar electric field is set up, and a steady state distribution along the magnetic field can be derived for a multispecies plasma. Thus, the local plasma properties measured at the spacecraft can be extrapolated along the magnetic field to the centrifugal equator.

3.1. Density Profiles at the Centrifugal Equator

In the Appendix of Paper 2 we show the procedure we used based on diffusive equilibrium in a rotating magnetic field [*Bagenal*, 1994]. We use a magnetic field model that combines the internal sources of the VIP4 model of *Connerney et al.* [1998] plus the field associated with an azimuthally symmetric equatorial current from *Connerney et al.* [1981], which we call VIP4 + CAN. We trace the magnetic field from the location of the spacecraft at the time of each measurement and find the centrifugal equator—the location farthest from Jupiter's spin axis. We then take the local measurements and extrapolate the plasma properties to the centrifugal equator.

Figure 6 shows the radial profiles of the local proton density measured at the spacecraft location and the density at the centrifugal equator of H^+ ions that have been derived by extrapolating the local measurements along the magnetic field under the assumption of diffusive equilibrium. From 6 to 12 R_J these profiles look pretty similar to the in situ profiles. Beyond about 12 R_J the spacecraft made larger excursions from the equator and the magnetic field deviates from a simple dipole due to equatorial currents. We cut off the centrifugal profile at about 16 R_J and fit empirical power law functions versus distance along the centrifugal equator ($\rho_{centrifugal}$) to the density profile (gray line). Beyond 16 R_J we used the shape of an empirical fit to Galileo and Voyager density data derived by *Bagenal and Delamere* [2011] and scaled the value to match at 15.2 R_J (blue line). The constants associated with the empirical functions for H^+ are given in Table 3. The function constants for the heavy ion species are given in Tables 2 and 3 of Paper 2. While the heavy ions show wild excursions of high density in the cold blob regions (see Paper 2) the protons are excluded by the ambipolar electric field from the equatorial region. Hence, the extrapolated equatorial profile of protons (blue dots) shows sharp dips in density in these cold blobs. We ignore these wild excursions in deriving an average profile.

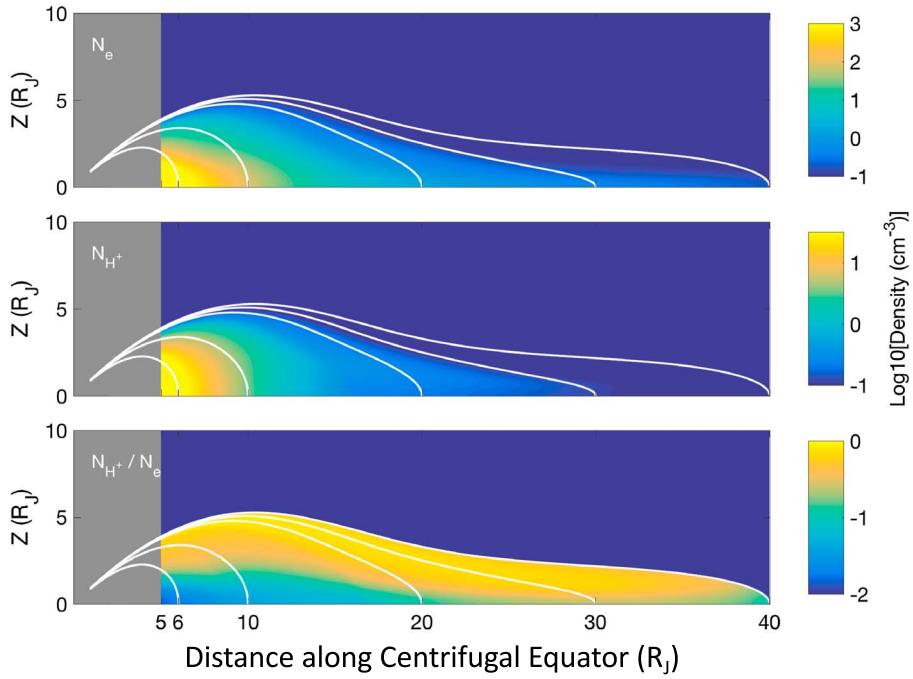

Figure 7. Contour plots of electron density (N_e), proton density (N_{H+}), and the ratio of N_{H+}/N_e in the plane of the magnetic field for the System III longitudes (110.8° and 290.8°) where the rotational, magnetic, and centrifugal equators align. The magnetic field lines are derived from the VIP4 + CAN magnetic field model.

3.2. Two-Dimensional Map of Protons

Assuming the plasma is distributed along the field in diffusive equilibrium, we can make a 2-D map of plasma properties from the plasma properties along the centrifugal equator. Figure 7 shows the map of electron density, proton density, and the ratio of protons to electrons. At two longitudes (System III = 110.8°, 290.8°) the Jovigraphic, magnetic, and centrifugal equators align. We picked these longitudes and used the empirical functions of density, temperature, and flow speed to derive two-dimensional maps of the plasma in the $\rho_{centrifugal} - Z_{centrifugal}$ plane. The maps have been truncated at 5 R_J radial distance and latitude of 35°.

Close to the equator, the vertical distribution of electrons is controlled by the dominant heavy ions (i.e., O^+ and S^{++}). The lighter protons are lifted off the equator by the ambipolar electric field and peak off the equator. Inside ~6 R_J the plasma rapidly cools and becomes tightly confined to the equator. To make the density map, we used the values of the local plasma properties extrapolated to the centrifugal equator. The extrapolation is fine when the spacecraft is close to the centrifugal equator (7 to 5.2 R_J for Voyager 1), but inside ~5 R_J, the scale height of the cold plasma is so small that extrapolation is very sensitive to the magnetic field model applied (see discussion in *Bagenal* [1994]).

4. Discussion: Sources of Minor Species

4.1. Sources of H^+

The solar wind, Jupiter's ionosphere, and the icy moons are all potential sources of protons found in the Jovian Magnetosphere. The relative importance of these different proton sources is not so easy to determine from just the spatial distribution of density and temperature of protons in the equatorial region. Figure 4 shows the density of protons dropping steeply with distance beyond 6 R_J, with the abundance relative to electrons at 2–3% in the torus (though the uncertainties in these numbers are fairly large given the very broad nature of the PLS spectra), rising up to ~20–30% at places within the plasma sheet beyond ~12 R_J. The temperature profile also follows the heavy ion profile except much more variable beyond ~15 R_J. There are places where the protons can be up to a factor of 10 warmer or colder than the heavy ions. Whether this implies different sources versus heating/cooling processes is not clear. Inside 6 R_J the density

and temperature of protons drops in a similar fashion to the heavy ions (see Figure 1 of Paper 2) with the dramatic differences in outbound versus inbound abundances likely due to protons being excluded from the centrifugal equator (inbound) and hence being enhanced away from the equator (outbound).

Sometimes ion composition is easier to distinguish at higher energies. *Hamilton et al.* [1981] summarized the Voyager Low-Energy Charged Particles (LECP) measurements at higher energies (~1 MeV/nucleon) that there was a clear signature of H_3^+ ions which clearly come from the ionosphere. The instruments on the Ulysses spacecraft were designed to measure the composition of the solar wind, but the gravity assist flyby of Jupiter in February 1992 was an opportunity to measure the composition within the magnetosphere of Jupiter. The presence of H_3^+ ions was corroborated by *Lanzerotti et al.* [1993] with Ulysses measurements at >50 keV. Reporting on measurements in the energy/charge range of 600 V to 60 kV, *Geiss et al.* [1992] showed that the Solar Wind Ion Composition Spectrometer instrument found roughly constant proton counts throughout the magnetosphere but noted that the counts of He^{++} (presumably from the solar wind) dropped significantly from 100 R_J to 20 R_J. *Mall et al.* [1993] argued that a high H^+/He^{++} ratio suggests a predominately ionospheric source for light ions in the magnetosphere. Similarly, *Keppler and Krupp* [1996] showed that the charge state of helium ions is around 1 between 10 and 50 R_J, increasing to 1.5–1.75 between 80 and 100 R_J. This would suggest an ionospheric source of He^+ in the inner magnetosphere, mixed with increasing solar wind He^{++} in the outer magnetosphere.

4.1.1. Solar Wind Source

The Voyager PLS data do not allow separation of light ions in the magnetosphere so we assume they are all protons. It might be tempting to take the increase in proton abundance with distance shown in Figure 4 as an indication of increasing contribution of solar wind protons. The problems with this argument are (1) our farthest measurements at nearly 30 R_J are still only 30–50% the distance to the dayside magnetopause (average location 60–90 R_J according to *Joy et al.* [2002]) and (2) it is hard to see how a solar wind source could produce the very cold protons sometimes observed in the plasma sheet. By comparison, the case for a significant solar wind source at Saturn is more convincing. *Thomsen et al.* [2010] report that at Saturn the ratio of protons to heavy ions increases all the way out to the magnetopause distance of ~20 R_S, ramping up outside ~15 R_S.

Hill et al. [1983] estimated the solar wind source by taking ~0.1% of incoming solar wind flux leaking into the magnetosphere, a radius of cross section of 100 R_J, and obtained a small source strength of 20 kg/s. *Bagenal and Delamere* [2011] took a more realistic cross section of the terminator of 150 R_J, a 1 cm^{-3} solar wind density, speed of 400 km/s, and estimated a solar wind mass flux of ~230 t/s which, using Hill's 0.1% leakage rate, makes a source of 230 kg/s.

Of course, the 0.1% leakage rate is just a rough estimate (based on experience at Earth). It is quite possible that the magnetopause is more permeable at Jupiter. The high plasma beta inside the magnetosphere makes it more responsive to changes in the solar wind pressure [*Joy et al.*, 2002], while a strong change in beta across the magnetopause suppresses large-scale reconnection [*Swisdak et al.*, 2003, 2010]. The strong flow shear across the magnetopause [*Galopeau et al.*, 1995] and field orientations on either side [*Desroche et al.*, 2012] indicate that the prevalence of shear-driven Kelvin-Helmholtz instabilities are likely stronger at Jupiter's magnetopause (see review by *Delamere et al.* [2015]). Strong K-H shears would drive small-scale intermittent reconnection, developing a boundary layer with substantial mixing of plasmas from either side.

Krupp et al. [2004] discussed evidence of a boundary layer seen in the Cassini Magnetosphere Imaging Instrument/Low Energy Magnetospheric Measurement System energetic electron data when Cassini skimmed Jupiter's dusk magnetopause during the gravity assist flyby. They suggest that the leakage of energetic magnetospheric electrons to the magnetosheath is consistent with open field lines inside the magnetopause. More recently, the particles measured by New Horizons as it traversed far down the flanks of the duskside magnetotail were increasingly dominated by light ions at farther distances down tail with different groups presenting arguments for these light ions coming from Jupiter [*McComas et al.*, 2007, 2017] versus leaking in from the solar wind [*Haggerty et al.*, 2009; *Hill et al.*, 2009; *Ebert et al.*, 2010]. NASA's Juno spacecraft is in a polar, 53 day orbit that means the spacecraft spends many weeks on the dawn flanks of Jupiter's magnetosphere. Hopefully, this will allow the capable Juno instruments to explore boundary processes as well as measure the interchange of solar wind and magnetospheric plasmas.

4.1.2. Ionospheric Source

Prespacecraft expectations of the magnetosphere of Jupiter were based on experience at Earth as well as observations of Jupiter's strong radio emissions (reviewed by *Carr et al*. [1983]). In two classic studies of comparative magnetospheres, *Brice and Ioannidis* [1970] showed that Jupiter's strong magnetic field and the weaker solar wind and magnetic field at 5 AU would mean that most of the inner magnetosphere would be coupled to the planet's rotation (i.e., mostly plasmasphere) with little solar wind driven convection. *Ioannidis and Brice* [1971] argued that photoelectrons would escape Jupiter's atmosphere and pull ~10^{26} protons per second from the ionosphere into the magnetosphere where they would gain ~1–3 keV of centrifugal energy. They suggested that the density of plasma in the magnetosphere would be limited by recombination, making a donut of plasma peaking with a density of ~100 cm^{-3} at about 8 R_J. *Swartz et al.* [1975] increased the escape flux to ~3×10^{27} s^{-1}.

After Voyager's detection of Io's volcanism and the dense Io plasma torus, the potential source of plasma from Jupiter's ionosphere was largely ignored. *Thorne* [1981] argued that if Jupiter's intense (~3×10^{13} W) aurora were caused by precipitating energetic (500 keV) heavy ions, then such energy deposition might enhance the ionospheric escape to 0.6–3×10^{28} s^{-1}, comparable to the iogenic plasma production rate by number but a mere 35 kg/s by mass. *Nagy et al.* [1986] applied early models of the polar wind developed for Earth to the ionosphere of Jupiter and explored how the escape rate of ionospheric protons and electrons depends on the abundance and temperature of a suprathermal electron population. *Nagy et al.* [1986] showed that suprathermal electrons could produce an escape flux of 2×10^{28} s^{-1}. While no one has further modeled the ionospheric outflow at Jupiter, *Glocer et al.* [2007, 2009] modeled potential ionospheric outflow at Saturn with a multifluid numerical model of the physical chemistry of the ionosphere-exosphere and estimated the source of H^+ and H_3^+ ions to be between 2×10^{26} and 8×10^{27} s^{-1}. The time is clearly ripe for such a model to be applied to Jupiter.

Radio emission from Jupiter has been monitored since the 1950s and provides valuable diagnostics about magnetospheric properties (see review by *Carr et al*. [1983]). Limits on the electron density of <10 cm^{-3} at high latitudes were first derived from the Faraday rotation of the radio waves [*Parker et al*., 1969] as well as from their elliptical polarization [*Melrose and Dulk*, 1991]. Another method is to model the frequency dispersion of whistler waves that travel along the magnetic field from Jupiter's ionosphere. *Tokar et al.* [1982a, 1982b] applied the Voyager PLS torus model of *Bagenal and Sullivan* [1981] to the dispersion of whistlers observed by Voyager plasma wave to derive a proton density outside the torus of 1–20 cm^{-2} and a source of $2.5 \times 10^{27\pm1}$ s^{-1}. *Crary et al.* [1996] updated the torus model of *Bagenal* [1994] to include thermal anisotropy and suprathermal tails for the ions and found off-equator proton densities 7–50 cm^{-3}.

Let us approximate the protons we see in the torus and plasma sheet in Figure 4 to be an average abundance of 10% of the total electron density. We then assume that this reflects an ionospheric source that has mixed with the torus plasma and transported out at the same rate as the heavy ions. We take the mass production rate of the torus of *Bagenal and Delamere* [2011] of 600–3000 kg/s, convert to 1.5–7.5×10^{28} s^{-1} and, after dividing by 10, get a proton production rate of 1.5–7.5×10^{27} protons s^{-1} (2.5–13 kg/s). This is considerably less than the 2×10^{28} protons s^{-1} of *Nagy et al.* [1986], comparable to the *Tokar et al.* [1982a, 1982b] estimate. We hope that the polar passes by Cassini at Saturn and the Juno mission to Jupiter will make direct measurements of the amount of outflowing ionospheric material from these gas giant planets.

4.1.3. Icy Satellite Source

In addition to the solar wind and ionosphere, there remains a third potential source of protons in the Jovian magnetosphere: the icy satellites. Of particular interest is the possibility that Europa's atmosphere, perhaps augmented by erupting plumes, might be a source of plasma. *Lagg et al.* [2003] observed depletions of the protons fluxes (80–200 keV) in Galileo European Pollen Database measurements around Europa's orbit which they explained by the presence of an extended neutral cloud with a density of 20–50 cm^{-3}. But they could not identify the composition of the neutrals. The Cassini INCA instrument detected fluxes of energetic neutral atoms from which *Mauk et al.* [2003] inferred the presence of a neutral cloud of unknown composition extending close to the orbit of Europa with a local density 40 cm^{-3}. Since the Cassini UVIS instrument did not detect UV emissions from neutral oxygen, *Hansen et al.* [2005] put an upper limit on the neutral oxygen density 8 cm^{-3}. One concludes, therefore, that the extended neutral cloud around Europa's orbit must be mostly hydrogen. At Europa's orbital distance of 9.4 R_J, the density of the plasma is too low for there to be significant

collisions. This means that any proton source from a Europa neutral cloud would be via photoionization (rather than electron impact ionization or CHEX) and likely weak compared with the ionospheric source. But there are few models of the interaction of the plasma with Europa's atmosphere that include the necessary chemistry to predict the neutral cloud and plasma sources [*Saur et al.*, 1998; *Dols et al.*, 2016]. With the possibility of future missions to Europa this is likely a productive area of research in the next few years.

4.2. Sources of Sodium Ions

Neutral sodium is relatively easy to observe because of its efficient scattering of visible sunlight. There have been extensive studies, therefore, of the morphology and variability of the sodium neutral cloud (reviewed by *Thomas et al.* [2004] and *Schneider and Bagenal* [2007]). In situ detection of sodium ions was first made with the Voyager LECP instrument at MeV energies by *Hamilton et al.* [1981] who reported a Na/O ratio of about 5%. How sodium from Io gets to such energies is not clear. At six orders of magnitude lower energy, the Voyager PLS data in the cold torus analyzed by *Bagenal and Sullivan* [1981] and *Bagenal* [1985] put an upper limit of the abundance at 3% for few eV Na^+ ions. *McNutt* [1993] makes the case for detection of Na^+ ions in a Voyager PLS measurement at 42 R_J, and the following year, *Hall et al.* [1994] report a tentative detection of Na^+ emission in the UV (~372 Å) from the torus. All reports are similar to our results that show the Na^+/N_e abundance between 1 and 10% from ~5 R_J in the cold torus to ~40 R_J in the plasma sheet.

The extensive modeling of the neutral sodium cloud suggests that the source is a combination of direct sputtering of Na from the atmosphere and some combination of charge exchange ($Na^+ + Y \rightarrow Na + Y^+$) or dissociative recombination ($NaX^+ + e^- \rightarrow X + Na$) where Y is SO_2 or a dissociated product thereof and X is likely Cl, S, or O [*Wilson et al.*, 2002; *Schneider and Bagenal*, 2007]. *Smyth and Combi* [1997] estimate that the total production of sodium into the neutral cloud is $3–25 \times 10^{26}$ s^{-1} (12–100 kg/s). *Bagenal and Delamere* [2011] estimate the range of plasma production in the torus to be 600–3000 kg/s. This means that few percent abundance of Na^+ is consistent with the eventual full ionization of the neutral clouds. *Mendillo et al.* [2004] showed that over ~7 years the sodium production varied proportionally with changes in IR emissions from Io, indicating that the sodium source is modulated by Io's volcanic activity. Similarly, *Brown and Bouchez* [1997] showed an increase in torus S^+ emission shortly after an increase in neutral Na emission. Similar variations in sodium emission with volcanic eruptions are reported by *Yoneda et al.* [2009, 2010, 2015]. The Io torus UV emissions observed by UVIS as Cassini approached Jupiter in 2000 showed factor ~3 variations following a volcanic eruption [*Delamere et al.*, 2004]. Nevertheless, while these rough numbers are consistent, there remain many questions about the similarities and differences in the details of the production and loss mechanisms for sodium and SO_2 products.

4.3. Sources of Sulfur Dioxide Ions

Positive identification of SO_2^+ ions is limited to 5.31 to 5.07 R_J. The local densities range from 1.6 to 9.3 cm^{-3}, corresponding to abundances of SO_2^+ ions in the range 0.1% to 0.6% of the local electron density. *Bagenal* [1985] found similar parameters for SO_2^+ ions. In the 1980s there was considerable discussion about what gases were escaping from Io (S_2 versus SO_2), whether the atmospheric loss was via sputtering, ionization, or charge exchange, and the relative importance of molecular versus atomic species in the plasma source. *Bagenal* [1985] examined the options of increasing the temperature of SO_2^+ ions (to 6 eV) or adding small amounts of SO^+ and SO_3^+ ions. In our reanalysis we found that adding a few percent of hot (Maxwellian, ~100 eV) O^+ ions in addition ~half a percent of SO_2^+ made a better match to the spectrum (Figure 3).

The Galileo flybys of Io produced further indication of molecular ions via the ion cyclotron waves measured by the magnetometer [*Kivelson et al.*, 1996]. On ionization, the fresh ions form a ring beam velocity distribution that is unstable to ion cyclotron wave emission. While the Galileo magnetometer measurements suggest the presence of SO_2^+, SO^+, and S^+ pickup ions, using these magnetic waves to determine the local densities and/or net production rate depends on details of the wave-particle physics [*Huddleston et al.*, 1997, 1998; *Cowee et al.*, 2008]. *Frank and Paterson* [2000] analyzed in situ plasma data from the Galileo I24 flyby of Io which they modeled with pickup ions of O^+, S^+, and SO^+, but no SO_2^+. Unfortunately, the Galileo PLS instrument did not have the spectral resolution to show definitive spectral signatures.

We find that we are able to match the spectrum with ion distributions that have equilibrated to Maxwellians at a common, cold temperature with just a few percent hot ions, also Maxwellian (Figure 3). Thus, the plasma

that has reached ~5.3 R_J in the cold inner torus seems to have evolved close to thermal equilibrium, both between species and within each species. Even the electrons could be equilibrated with the ions [*Sittler and Strobel*, 1987]. The exception is the few percent populations of ~100 eV hot ions which we fit as O^+ ions but could be some combination of different ions (including small amounts of SO^+, S_2^+, and SO_3^+). The apparent Maxwellian nature of these hot ions suggests that they might be either pickup ions which have thermalized within the species but not equilibrated with the rest of the plasma. Alternatively, a suprathermal population could have diffused in from the warm torus and cooled (e.g., through Coulomb collisions with the dense, cold thermal plasma) but not reached full equilibrium.

Observations by Voyager UVS [*Shemansky*, 1980] and Galileo PLS [*Bagenal*, 1997] suggest that less than ~20% of the ~1 t/s plasma source is produced locally near Io. Detection of emissions from neutral clouds of atomic oxygen [*Brown*, 1981] and sulfur [*Durrance et al.*, 1983] supported the idea of the torus being supplied by ionization of a roughly uniform ring of neutral atoms at Io's orbital distance. Physical chemistry models applying entirely atomic (rather than molecular) chemistry to the neutral clouds [*Smyth and Marconi*, 2003] and the torus [*Delamere and Bagenal*, 2003] could match the remote and in situ observations with neutral atomic O and S escaping from Io at a net rate of ~2×10^{28} s^{-1} with O/S~2, consistent with the dissociation of SO_2. Thus, it seemed that SO_2^+ ions were exotic but played an insignificant role.

Interest in a potentially significant role of SO_2 was provoked by the results of modeling the plasma interaction with Io's atmosphere by *Dols et al.* [2008, 2012] which included the chemistry of the multispecies torus interacting with both molecular and atomic species in the atmosphere.

4.3.1. Ionization of the Atmosphere

Dols et al. [2008] estimate that the net plasma production is ~200 kg/s of SO_2^+, ~70 kg/s of SO^+, and ~20 kg of S^+ for the conditions during Galileo's first Io flyby when the density was high (n_e ~ 4000 cm^{-3}). While most of this production is electron impact ionization by the thermal plasma flowing into the atmosphere, *Saur et al.* [2002] and *Dols et al.* [2008] both note that suprathermal (>20 eV) electrons, which stream along the magnetic field, also contribute to ionization of atmospheric SO_2.

4.3.2. Charge Exchange of S and O Ions with Atmospheric SO_2

Dols et al. [2008] also showed that charge exchange (CHEX) reactions between the incoming S^{n+} and O^{n+} ions (where n = 1 to 3 for ions of increasing charge state) with neutral SO_2 quickly produces a further ~10 kg/s of SO_2^+ ions and reduces the plasma to lower charge state. Eventually, the sulfur and oxygen ions become neutral atoms which have retained much of their original speed but are no longer confined by Jupiter's magnetic field. These CHEX reactions are removing ~30 kg/s of the incoming S^{n+} and O^{n+} ions. Neutralized material on the outer regions of the interaction region are moving at a speed close to corotation with Jupiter (~75 km/s at Io's orbit) and escape the system as energetic neutral atoms at ~250 and ~500 eV for O and S, respectively. Material neutralized closer to Io, where the flow has been slowed down in the electrodynamic interaction, will spread out in a neutral cloud around Io's orbit.

4.3.3. Resonant SO_2 Charge Exchange

The substantial amount of SO_2^+ ions produced via electron impact ionization and CHEX are accelerated up to the local plasma flow speed. These SO_2^+ ions can undergo further (resonant) CHEX with the neutral background, producing SO_2 molecules at higher energies than the background atmosphere, spreading the outer atmosphere and, if they have enough energy, escaping to feed the extended neutral cloud of SO_2, perhaps escape the Jupiter system. *Dols et al.* [2008, 2012] show that this resonant CHEX process is the main contributor to atmospheric loss.

4.3.4. Dissociation of SO_2

The threshold energy for electron impact dissociation of SO_2 is relatively low (5.7 eV) so that electrons in the incoming plasma (Te ~ 5 eV) efficiently dissociate the SO_2 into SO and O neutral fragments. These fragments are usually slow (~1 eV) [*Vatti Palle et al.*, 2004] and feed an O and S neutral corona. *Dols et al.* [2008, 2012] point out that the SO_2^+ ions produced in the interaction that reach the dense, cold wake behind Io will dissociatively recombine in ~1 h, reducing the plasma source but contributing neutral fragments to Io's surroundings. *Dols et al.* [2012] estimate that 1.5 t/s of dissociation products could feed the neutral clouds around Io's orbit.

Dols et al. [2012] extended the modeling of the plasma interaction by making Io's atmosphere nonuniform in both latitude and longitude, with the goal of matching the plasma perturbations observed on multiple flybys

of Io. From the five different flybys over 1995–2001 it is hard to tell if the atmosphere is permanently nonuniform or varies over time. Perhaps the most important result from *Dols et al.* [2008] is the suggestion that 2–3 t/s of fast SO_2 molecules are produced via CHEX and spread out into the Jupiter system.

Thus, it seems possible that the interaction with Io's atmosphere provides little plasma directly (as noted by *Shemansky* [1980] and *Bagenal* [1997]) but makes ~1.5 t/s of O and S atoms that spread out around Jupiter, making the extending atomic source, consistent with the models of *Smyth and Marconi* [2003] and *Delamere and Bagenal* [2003]. But the details are important. Some combination of the multiple processes (ionization, dissociation, and CHEX) occurring between the incoming multispecies plasma and the predominately SO_2 (but also with SO, S, and O in the upper layers) atmosphere of Io need to produce neutrals that are not too slow that they cannot escape Io and not too fast that they escape Jupiter. Furthermore, observations of the neutral O and S clouds are very sparse and an extended neutral cloud of SO_2 may not be detectable. Who knew SO_2 chemistry could be so complicated.

5. Summary and Conclusions

We explore the distribution of minor ions in the Io torus and plasma sheet of Jupiter's magnetosphere based on a reanalysis of Voyager 1 and 2 PLS ion data obtained in March and July 1979. The data set and analysis method is described in Paper 1 [*Bagenal et al.*, 2017], and the dominant, heavy (S^{n+} and O^{n+}) ion distributions are described in Paper 2 [*Dougherty et al.*, 2017]. In this paper we present the analysis of three minor ions—H^+, Na^+, and $SO_2{}^+$—which we summarize as follows:

1. Protons comprise 1–20% of the plasma between 5 and 30 R_J. They exhibit temperatures that vary by a factor of 10 warmer or colder than the heavy ions. From the distribution of proton densities and temperatures in the torus and plasma sheet we are not able to come to firm conclusions about the source of these protons, except that their location deep within the magnetosphere is most consistent with an ionospheric source of ~1.5–7.5 × 10^{27} protons s^{-1} (2.5–13 kg/s).
2. Sodium ions are detected by the Voyager PLS instrument between 5 and 40 R_J at an abundance of 1 to 10%. These Na^+ ions are mostly likely from the ionization of the extended neutral cloud emanating from Io that has been observed since *Brown* [1974]. While the neutral sodium cloud has been extensively monitored and correlated with volcanic activity, from ground-based telescopes via the strong optical emissions, the relationship between the physical processes that produce the sodium neutral cloud and ion population is not easily related to the processes governing the SO_2 products.
3. Sulfur dioxide ions are detected by the Voyager PLS instrument between 5.31 and 5.07 R_J at an abundance of 0.1–0.6%. These $SO_2{}^+$ ions clearly come from the plasma interaction with Io's atmosphere, but the exact processes whereby atmospheric molecules escape Io and end up as ions well inside Io's orbit are not clear.

In the 38 years since the Voyager 1 and 2 flybys of Jupiter there have been major advances in our understanding of the system. But fundamental questions remain. In this paper we argue that evaluating the roles of minor ions could play useful roles. The two major issues seem to be (1) What is the source of light ions from Jupiter's atmosphere/ionosphere? (2) How does the interaction of plasma with Io's atmosphere produce the extensive neutral clouds around Io's orbit and the ~t/s plasma that supplies the Io plasma torus? The expectation is that Juno, in a polar orbit around Jupiter, will answer question (1) about the proton production from Jupiter's atmosphere.

Regarding question (2) about the Io interaction and the Io torus, there are some recent developments: (i) Models suggest that ~90% of the plasma moves *outward* from Io [e.g., *Delamere et al.*, 2005], but we see the peak density in a "ribbon" extending *inside* Io's orbit. (ii) Adding to known neutral clouds of atomic O and S, Galileo observations and models show molecular SO_2 and SO are also key [*Huddleston et al.*, 1997, 1998; *Dols et al.*, 2008, 2012]. (iii) Reanalysis of Voyager observations of $SO_2{}^+$ ions quantifies their distribution inside Io's orbit.

These recent studies show that we need a quantitative model of the Io-neutral-plasma system to answer specific questions about the Io plasma torus: (a) What shapes the neutral clouds (molecular and atomic) produced by the interaction of torus plasma with Io's atmosphere? What are the similarities and differences between the sources and losses of SO_2 (and dissociation products) and the processes governing sodium? How much is escape of O, S produced in the atmosphere by electron impact [*Smyth and Marconi*, 2003]

versus electron impact on an extended cloud of SO_2 versus dissociative recombination of SO_2^+ ions away from Io [*Dols et al*., 2008, 2012]? (b) Why does the production of plasma peak well inside Io's orbit? What makes "the ribbon"? (c) What happens to the cold torus material that diffuses inward from Io? (d) Could the flux of fast escaping neutrals from charge exchange reactions provide a significant source (via photoionization) in the outer magnetosphere? We anticipate a productive future exploring these issues with increasingly sophisticated models and new data.

Acknowledgments
We thank John Belcher and John Richardson for their assistance in accessing the PLS and trajectory data and with translation of the original analysis code. The diligent archiving of PLS documentation by Ralph McNutt is gratefully appreciated. We thank Vincent Dols and Nick Schneider for their comments. The raw Voyager PLS data are archived in the Planetary Data System (PDS—https://pds.nasa.gov/). We have gathered the data for the Jovian magnetosphere, the fitting routines, output of our analysis, and comparisons with previous analyses of these data, here: http://lasp.colorado.edu/home/mop/missions/voyager. We acknowledge support from NASA's Jupiter Data Analysis Program (NNX09AE03G) as well as the Juno mission (SWRI subcontract 699050X).

References

Bagenal, F. (1985), Plasma conditions inside Io's orbit: Voyager measurements, *J. Geophys. Res.*, *90*, 311–324, doi:10.1029/JA090iA01p00311.
Bagenal, F. (1994), Empirical model of the Io plasma torus: Voyager measurements, *J. Geophys. Res.*, *99*, 11,043–11,062, doi:10.1029/93JA02908.
Bagenal, F. (1997), The ionization source near Io from Galileo wake data, *Geophys. Res. Lett.*, *24*, 2111–2114, doi:10.1029/97GL02052.
Bagenal, F., and P. A. Delamere (2011), Flow of mass and energy in the magnetospheres of Jupiter and Saturn, *J. Geophys. Res.*, *116*, A05209, doi:10.1029/2010JA016294.
Bagenal, F., and J. D. Sullivan (1981), Direct plasma measurements in the Io torus and inner magnetosphere of Jupiter, *J. Geophys. Res.*, *86*, 8447–8466.
Bagenal, F., L. P. Dougherty, K. M. Bodisch, J. D. Richardson, and J. M. Belcher (2017), Survey of Voyager plasma science ions at Jupiter: 1. Analysis method, *J. Geophys. Res. Space Physics*, *122*, doi:10.1002/2016JA023797.
Brice, N. M., and G. A. Ioannidis (1970), The magnetospheres of Jupiter and Earth, 347, *Icarus*, *13*(2), 173–183, doi:10.1016/0019-1035(70)90048-5.
Bridge, H. S., J. W. Belcher, R. J. Butler, A. J. Lazarus, A. M. Mavretic, J. D. Sullivan, G. L. Siscoe, and V. M. Vasyliunas (1977), The plasma experiment on the 1977 Voyager mission, *Space Sci. Rev.*, *21*, 259–287.
Brown, R. A. (1974), Optical line emission from Io, in *Exploration of the Planetary System*, edited by A. Woszczyk and C. Iwaniszewska, 527 pp., D. Reidel, Dordrecht, Netherlands.
Brown, R. A. (1981), The Jupiter hot plasma torus—Observed electron temperature and energy flows, *Astrophys. J.*, *244*, 1072–1080.
Brown, M., and A. Bouchez (1997), The response of Jupiter's magnetosphere to a volcanic outburst on Io, *Science*, *278*, 268–271.
Carr, T., M. Desch, and J. Alexander (1983), Phenomenology of magnetospheric radio emissions, in *Physics of the Jovian Magnetosphere*, edited by A. J. Dessler, pp. 226–284, Cambridge Univ. Press, Cambridge.
Connerney, J. E. P., M. H. Açuna, and N. F. Ness (1981), Modeling the Jovian current sheet and inner magnetosphere, *J. Geophys. Res.*, *86*, 8370–8384.
Connerney, J. E. P., M. H. Acuña, N. F. Ness, and T. Satoh (1998), New models of Jupiter's magnetic field constrained by the Io flux tube footprint, *J. Geophys. Res.*, *103*, 11,929–11,939.
Cowee, M. M., C. T. Russell, and R. J. Strangeway (2008), One-dimensional hybrid simulations of planetary ion pickup: Effects of variable plasma and pickup conditions, *J. Geophys. Res.*, *113*, A08220, doi:10.1029/2008JA013066.
Crary, F. J., F. Bagenal, J. A. Ansher, D. A. Gurnett, and W. S. Kurth (1996), Anisotropy and proton density in the Io plasma torus derived from whistler wave dispersion, *J. Geophys. Res.*, *101*, 2699–2706.
Delamere, P., and F. Bagenal (2003), Modeling variability of plasma conditions in the Io torus, *J. Geophys. Res.*, *108*(A7), 1276, doi:10.1029/2002JA009706.
Delamere, P., A. Steffl, and F. Bagenal (2004), Modeling temporal variability of plasma conditions in the Io torus during the Cassini era, *J. Geophys. Res.*, *109*, A10216, doi:10.1029/2003JA010354.
Delamere, P., F. Bagenal, and A. Steffl (2005), Radial variations in the Io plasma torus during the Cassini era, *J. Geophys. Res.*, *110*, A12223, doi:10.1029/2005JA011251.
Delamere, P. A., F. Bagenal, C. Paranicas, A. Masters, A. Radioti, B. Bonfond, L. Ray, X. Jia, J. Nichols, and C. Arridge (2015), Solar wind and internally driven dynamics: Influences on magnetodiscs and auroral responses, *Space Sci. Rev.*, *187*, 51–97, doi:10.1007/s11214-014-0075-1.
Desroche, M., F. Bagenal, P. A. Delamere, and N. Erkaev (2012), Conditions at the expanded Jovian magnetopause and implications for the solar wind interaction, *J. Geophys. Res.*, *117*, A07202, doi:10.1029/2012JA017621.
Dols, V. J., P. A. Delamere, and F. Bagenal (2008), A multispecies chemistry model of Io's local interaction with the plasma torus, *J. Geophys. Res.*, *113,* A09208, doi:10.1029/2007JA012805.
Dols, V. J., P. A. Delamere, F. Bagenal, W. S. Kurth, and W. R. Paterson (2012), Asymmetry of Io's outer atmosphere: Constraints from five Galileo flybys, *J. Geophys. Res.*, *117*, E10010, doi:10.1029/2012JE004076.
Dols, V. J., F. Bagenal, T. A. Cassidy, F. J. Crary, and P. A. Delamere (2016), Europa's atmospheric neutral escape: Importance of symmetrical O_2 charge exchange, *Icarus*, *264*, 387–397.
Dougherty, L. P., K. M. Bodisch, and F. Bagenal (2017), Survey of Voyager plasma science ions at Jupiter: 2. heavy ions, *J. Geophys. Res.*, in press.
Durrance, S. T., P. D. Feldman, and H. A. Weaver (1983), Rocket detection of ultraviolet emission from neutral oxygen and sulfur in the Io torus, *Astrophys. J.*, *267*, L125.
Ebert, R. W., D. J. McComas, F. Bagenal, and H. A. Elliott (2010), Location, structure, and motion of Jupiter's dusk magnetospheric boundary from ~625 to 2550 R_J, *J. Geophys. Res.*, *115*, A12223, doi:10.1029/2010JA015938.
Frank, L. A., and W. R. Paterson (2000), Return to Io by the Galileo spacecraft: Plasma observations, *J. Geophys. Res.*, *105*, 25,363–25,378, doi:10.1029/1999JA000460.
Galopeau, P. H. M., P. Zarka, and D. L. Quéau (1995), Source location of Saturn's kilometric radiation: The Kelvin-Helmholtz instability hypothesis, *J. Geophys. Res.*, *100*, 26,397–26,410.
Geiss, J., et al. (1992), Plasma composition in Jupiter's magnetosphere: Initial results from the solar wind ion composition spectrometer, *Science*, *257*, 1537–1539.
Glocer, A., T. Gombosi, G. Tóth, K. C. Hansen, A. J. Ridley, and A. Nagy (2007), Polar wind outflow model: Saturn results, *J. Geophys. Res.*, *112*, A01304, doi:10.1029/2006JA011755.
Glocer, A., G. Tóth, T. Gombosi, and D. Welling (2009), Modeling ionospheric outflows and their impact on the magnetosphere, initial results, *J. Geophys. Res.*, *114*, A05216, doi:10.1029/2009JA014053.
Haggerty, D. K., M. E. Hill, R. L. McNutt Jr., and C. Paranicas (2009), Composition of energetic particles in the Jovian magnetotail, *J. Geophys. Res.*, *114*, A02208, doi:10.1029/2008JA013659.

Hall, D. T., et al. (1994), Extreme ultraviolet explorer satellite observations of Jupiter's Io plasma torus, *Astrophys. J. Lett.*, *426*, L51–L54.
Hamilton, D. C., G. Gloeckler, S. M. Krimigis, and L. J. Lanzerotti (1981), Composition of nonthermal ions in the Jovian magnetosphere, *J. Geophys. Res.*, *86*, 8301–8318, doi:10.1029/JA086iA10p08301.
Hansen, C., D. E. Shemansky, and A. R. Hendrix (2005), Cassini UVIS observations of Europa's oxygen atmosphere and torus, *Icarus*, *176*, 305–315.
Hill, T. W., A. J. Dessler, and C. K. Goertz (1983), Magnetospheric models, in *Physics of the Jovian Magnetosphere*, edited by A. J. Dessler, pp. 353–394, Cambridge Univ. Press, New York, doi:10.1017/CBO9780511564574.012.
Hill, M. E., D. K. Haggerty, R. L. McNutt, and C. P. Paranicas (2009), Energetic particle evidence for magnetic filaments in Jupiter's magnetotail, *J. Geophys. Res.*, *114*, A11201, doi:10.1029/2009JA014374.
Huddleston, D. E., R. J. Strangeway, J. Warnecke, C. T. Russell, M. G. Kivelson, and F. Bagenal (1997), Ion cyclotron waves in the Io torus during the Galileo encounter: Warm plasma dispersion analysis, *Geophys. Res. Lett.*, *24*, 2143–2146, doi:10.1029/97GL01203.
Huddleston, D. E., R. J. Strangeway, J. Warnecke, C. T. Russell, and M. G. Kivelson (1998), Ion cyclotron waves in the Io torus: Wave dispersion, free energy analysis, and SO_2^+ source rate estimates, *J. Geophys. Res.*, *103*, 19,887–19,889.
Ioannidis, G., and N. Brice (1971), Plasma densities in the Jovian magnetosphere: Plasma slingshot or Maxwell demon, *Icarus*, *14*, 360–373.
Joy, S. P., M. G. Kivelson, R. J. Walker, K. K. Khurana, C. T. Russell, and T. Ogino (2002), Probabilistic models of the Jovian magnetopause and bow shock locations, *J. Geophys. Res.*, *107*(A10), 1309, doi:10.1029/2001JA009146.
Keppler, E., and N. Krupp (1996), The charge state of helium in the Jovian magnetosphere: A possible method to determine it, *Planet. Space Sci.*, *44*, 71–75.
Kivelson, M. G., K. K. Khurana, R. J. Walker, J. Warnecke, C. T. Russell, J. A. Linker, D. J. Southwood, and C. Polanskey (1996), Io's interaction with the plasma torus: Galileo magnetometer report, *Science*, *274*, 396–398, doi:10.1126/science.274.5286.396.
Krupp, N., J. Woch, A. Lagg, S. Livi, D. G. Mitchell, S. M. Krimigis, M. K. Dougherty, P. G. Hanlon, T. P. Armstrong, and S. A. Espinosa (2004), Energetic particle observations in the vicinity of Jupiter: Cassini MIMI/LEMMS results, *J. Geophys. Res.*, *109*, A09S10, doi:10.1029/2003JA010111.
Lagg, A., N. Krupp, J. Woch, and D. J. Williams (2003), In-situ observations of a neutral gas torus at Europa, *Geophys. Res. Lett.*, *30*(11), 1556, doi:10.1029/2003GL017214.
Lanzerotti, L. J., C. G. Maclennan, and D. M. Feldman (1993), Ulysses measurements of energetic H_3 molecules in Jupiter's magnetosphere, *J. Geophys. Res.*, *98*, 21,145–21,149.
Mall, U., J. Geiss, H. Balsiger, G. Gloeckler, A. B. Calvin, and B. Wilken (1993), Hydrogen from Jupiter's atmosphere in the Jovian magnetosphere, *Planet. Space Sci.*, *41*, 947–951.
Mauk, B. H., D. G. Mitchell, S. M. Krimigis, E. C. Roelof, and C. P. Paranicas (2003), Energetic neutral atoms from a trans-Europa gas torus at Jupiter, *Nature*, *421*, 920–921.
McComas, D. J., F. Allegrini, F. Bagenal, F. Crary, R. W. Ebert, H. Elliott, A. Stern, and P. Valek (2007), Diverse plasma populations and structures in Jupiter's magnetotail, *Science*, *318*, 217, doi:10.1126/science.1147393.
McComas, D. J., F. Allegrini, F. Bagenal, R. W. Ebert, H. A. Elliott, G. Nicolaou, J. R. Szalay, P. Valek, and S. Weidner (2017), Jovian deep magnetotail composition and structure, *J. Geophys. Res. Space Physics*, *122*, 1763–1777, doi:10.1002/2016JA023039.
McNutt, R. L., Jr. (1993), Possible in situ detection of K^{2+} in the Jovian magnetosphere, *J. Geophys. Res.*, *98*, 21,221–21,229.
McNutt, R. L., Jr., J. W. Belcher, and S. H. Bridge (1981), Positive ion observations in the middle magnetosphere of Jupiter, *J. Geophys. Res.*, *86*, 8319–8342.
Melrose, D. B., and G. A. Dulk (1991), On the elliptical polarization of Jupiter's decametric radio emission, *Astron. Astrophys.*, *249*, 250–257.
Mendillo, M., J. K. Wilson, J. Spencer, and J. Stansberry (2004), Io's volcanic control of Jupiter's extended neutral clouds, *Icarus*, *170*, 430–442.
Nagy, A. F., A. R. Barakat, and R. W. Schunk (1986), Is Jupiter's ionosphere a significant plasma source for its magnetosphere?, *J. Geophys. Res.*, *91*, 351–354, doi:10.1029/JA091iA01p00351.
Parker, G. D., G. A. Dulk, and J. W. Warwick (1969), Faraday effect on Jupiter's radio bursts, *Astrophys. J.*, *157*, 439–448.
Pearl, J., R. Hanel, V. Kunde, W. Maguire, K. Fox, S. Gupta, C. Ponnamperuma, and F. Raulin (1979), Identification of gaseous SO_2 and new upper limits for other gases on Io, *Nature*, *280*, 755–759.
Saur, J., et al. (1998), Interaction of the jovian magnetosphere with Europa: Constraints on the neutral atmosphere, *J. Geophys. Res.*, *103*, 19,947–19,962.
Saur, J., F. M. Neubauer, D. F. Strobel, and M. E. Summers (2002), Interpretation of Galileo's Io plasma and field observations: I0, I24, and I27 flybys and close polar passes, *J. Geophys. Res.*, *107*(A12), 1422, doi:10.1029/2001JA005067.
Schneider, N. M., and F. Bagenal (2007), Io's neutral clouds, plasma torus, and magnetospheric interaction, in *Io After Galileo*, edited by R. C. Lopes and J. R. Spencer, pp. 265–286, Springer, New York.
Scudder, J. D., E. C. Sittler Jr., and H. S. Bridge (1981), A survey of the plasma electron environment of Jupiter: A view from Voyager, *J. Geophys. Res.*, *86*, 8157–8179.
Shemansky, D. E. (1980), Mass-loading and diffusion-loss rates of the Io plasma torus, *Astrophys. J.*, *242*, 1266.
Sittler, E. C., Jr., and D. F. Strobel (1987), Io plasma torus electrons: Voyager 1, *J. Geophys. Res.*, *92*, 5741–5762.
Smyth, W. H., and M. R. Combi (1997), Io's sodium exosphere and spatially extended cloud: A consistent flux speed distribution, *Icarus*, *126*, 58–77.
Smyth, W. H., and M. L. Marconi (2003), Nature of the iogenic plasma source in Jupiter's magnetosphere I. Circumplanetary distribution, *Icarus*, *166*, 85.
Smythe, W. D., R. M. Nelson, and D. B. Nash (1979), Spectral evidence for SO_2 frost or adsorbate on Io's surface, *Nature*, *280*, 766.
Steffl, A. J., F. Bagenal, and A. I. F. Stewart (2004), Cassini UVIS observations of the Io plasma torus: II. Radial variations, *Icarus*, *172*, 91–103.
Swartz, W. E., R. W. Reed, and T. R. McDonough (1975), Photoelectron escape from the ionosphere of Jupiter, *J. Geophys. Res.*, *80*, 495–501.
Swisdak, M., B. N. Rogers, J. F. Drake, and M. A. Shay (2003), Diamagnetic suppression of component magnetic reconnection at the magnetopause, *J. Geophys. Res.*, *108*(A5), 1218, doi:10.1029/2002JA009726.
Swisdak, M., M. Opher, J. F. Drake, and F. Alouani Bibi (2010), The vector direction of the interstellar magnetic field outside the heliosphere, *Astrophys. J.*, *710*, 1769–1775, doi:10.1088/0004-637X/710/2/1769.
Thomas, N., F. Bagenal, T. Hill, and J. Wilson (2004), The Io neutral clouds and plasma torus, in *Jupiter: Planet, Satellites, Magnetosphere*, edited by F. Bagenal, T. E. Dowling, and W. B. McKinnon, pp. 561–591, Cambridge Univ. Press.
Thomsen, M. F., D. B. Reisenfeld, D. M. Delapp, R. L. Tokar, D. T. Young, F. J. Crary, E. C. Sittler, M. A. McGraw, and J. D. Williams (2010), Survey of ion plasma parameters in Saturn's magnetosphere, *J. Geophys. Res.*, *115*, A10220, doi:10.1029/2010JA015267.
Thorne, R. M. (1981), Jovian auroral secondary electrons and their influence on the Io plasma torus, *Geophys. Res. Lett.*, *8*, 509–512.

Tokar, R. L., et al. (1982a), Light ion concentrations in Jupiter's inner magnetosphere, *J. Geophys. Res.*, *87*, 2241.
Tokar, R. L., et al. (1982b), Proton concentration in the vicinity of the Io plasma torus, *J. Geophys. Res.*, *87*, 10,395–10,400.
Trafton, T., T. Parkinson, and W. Macy (1974), The spatial extent of sodium emission around Io, *Astrophys. J.*, *190*, L85.
Vatti Palle, P., J. Ajello, and A. Bhardwaj (2004), High-resolution far ultraviolet spectrum of electron-excited SO_2, *J. Geophys. Res.*, *109*, A02310, doi:10.1029/2003JA009828.
Wilson, J. K., M. Mendillo, J. Baumgardner, N. M. Schneider, J. T. Trauger, and B. Flynn (2002), The dual sources of Io's sodium clouds, *Icarus*, *157*, 476–489.
Yoneda, M., M. Kagitani, and S. Okano (2009), Short-term variation of Jupiter's extended sodium nebula, *Icarus*, *204*, 589–596.
Yoneda, M., H. Nozawa, H. Misawa, M. Kagitani, and S. Okano (2010), Jupiter's magnetospheric change by Io's volcanoes, *Geophys. Res. Lett.*, *37*, L11202, doi:10.1029/2010GL043656.
Yoneda, M., M. Kagitani, F. Tsuchiya, T. Sakanoi, and S. Okano (2015), Brightening event seen in observations of Jupiter's extended sodium nebula, *Icarus*, *261*, 31–33.